Materials Research Express

RECEIVED
27 June 2018

REVISED
1 August 2018

ACCEPTED FOR PUBLICATION
29 August 2018

PUBLISHED
7 September 2018

PAPER

Effect of cathode interface thickness on the photovoltaic parameters of bulk heterojunction organic solar cells

Minu Mohan and Manoj A G Namboothiry

School of Physics, Indian Institute of Science Education and Research Thiruvananthapuram (IISER-TVM), Thiruvananthapuram, 695551, India

E-mail: manoj@iisertvm.ac.in

Keywords: open-circuit voltage, built in potential, zinc oxide, organic bulk heterojunction solar cell

Supplementary material for this article is available online

Abstract

We investigate the role of cathode interfacial layer thickness in tuning the barrier height and charge transport in inverted bulk heterojunction organic solar cells (BHJ OSCs). The variation of cathode layer thickness significantly changed the cell parameters like open-circuit voltage (V_{oc}) and short-circuit current density (J_{sc}). For better understanding of the charge transport properties in the device, photoinduced capacitance spectroscopic studies and temperature dependent studies were carried out in polythieno[3,4-b]thio phene/benzodithiophene : [6,6]-phenyl-C71-butyric acid methyl ester (PTB7:$PC_{71}BM$) based inverted BHJ OSC with ZnO as the cathode interfacial layer. These studies gave insight into the charge accumulation and barrier height at the active layer/ZnO interface. Due to the presence of trap states in the ZnO layer, charges can accumulate at the interface creating a barrier for the smooth extraction of charge carriers. The barrier height is found to increase from 0.05 to 0.13 eV as the ZnO thickness is varied from 30 to 250 nm that can be attributed to the increase in the density of trap states in the ZnO layer. Intensity-dependent studies were also performed to analyze the recombination processes in the device.

Introduction

Recent developments in the field of organic bulk heterojunction (BHJ) solar cells makes it a promising technology to efficiently convert solar energy into useful electricity [1]. The research field has witnessed significant progress in enhancing the power conversion efficiency (PCE) of BHJ solar cells above 10% with the use of various device architectures and new materials [2–4]. The parameters like open-circuit voltage (V_{oc}), short-circuit current density (J_{sc}) and fill factor (FF) govern the efficiency of organic solar cells. Even in a highly efficient solar cells, the V_{oc} is usually less than the effective band gap (E_g) given by $|HOMO_{donor}\text{-}LUMO_{acceptor}|$, where $HOMO_{donor}$ is the highest occupied molecular orbital of donor and $LUMO_{acceptor}$ is the lowest unoccupied molecular orbital of the acceptor [5, 6]. Several factors like light intensity, temperature, recombination, and charge transfer states influence the V_{oc} value [7]. The surface and bulk recombination can further reduce the upper limit of V_{oc} by a factor of 3 eV [8–10]. Choosing an appropriate interfacial layer has a crucial role in reducing the interface recombination and thereby improving the V_{oc}.

Literature reports show that photogenerated charge carriers can accumulate at the interface between the active layer and the electrode leading to photovoltaic losses in the organic solar cells [11]. Buffer layers of proper energy band alignments on either side of the active layer are required for the efficient charge extraction and transportation of charge carriers to the respective electrodes, thereby increasing the efficiency of the solar cells. Specifically, for an inverted BHJ solar cell, the selection of electron transporting layer (ETL) has a vital role on the device performance [12, 13]. ETLs essentially need to be highly transparent for light to reach the active layer and at the same time electrically conductive. Considering these criteria, zinc oxide (ZnO) is a promising material as

an ETL. ZnO is a wide band gap semiconductor with large exciton binding energy, high electron mobility, and environmental stability [14, 15].

In this report, we focus on the effect of solution-processed ZnO layer thickness on the cell parameters of polythieno[3,4-b]thio phene/benzodithiophene: [6,6]-phenyl-C71-butyric acid methyl ester (PTB7:$PC_{71}BM$) based inverted BHJ organic solar cell. The presence of trap states and accumulation of charge carriers at the interfaces are investigated using photoinduced capacitance spectroscopic studies. The sum of the barrier height, determined from temperature dependent studies, exhibits variation with the cathode interface layer thickness. Intensity-dependent studies give insight into the role of the ZnO layer thickness in various recombination mechanisms in the device.

Experimental methods

Inverted BHJ solar cells were fabricated with the device architecture: ITO/ZnO/PTB7:$PC_{71}BM$/MoO_3/Ag in which ZnO is the electron transporting layer. ZnO nanoparticles solution was spin-coated on top of cleaned ITO coated glass plates. Multiple coatings were done to vary the ZnO layer thickness. The thickness of the ZnO films was measured using profilometer (Alpha-Step D-600 Stylus Profiler, KLA-Tencor) and was found to be 30, 70, 150 and 250 nm for 1, 3, 5 and 10 layers respectively. The detailed procedure of ZnO nanoparticles preparation is described elsewhere [16]. In brief, 23 mmol KOH solution in methanol (65 ml) was added dropwise to Zinc acetate dihydrate (13.4 mmol) in methanol (125 ml). The solution was stirred at 65 °C for 2.5 h and kept for overnight precipitation. The precipitate was washed twice with methanol and re-dispersed in a mixture of butanol (70 ml), methanol (5 ml) and chloroform (5 ml). On top of the ZnO layer, PTB7:$PC_{71}BM$ solution of 1:1.5 ratio is spin coated to form a 120 nm thick active layer. Hole transporting layer, MoO_3 (5 nm), and the back contact electrode, Ag (100 nm) were thermally evaporated at a low pressure of $\sim 10^{-6}$ Torr. The device area was 10 mm^2.

The current density-voltage (J-V) characteristics of the devices were carried out using a Keithley 6430 source meter under dark and illumination of 1000 Wm^{-2} AM1.5G spectrum using an Oriel 3A solar simulator tested with an NREL calibrated silicon solar cell. Light intensity dependent capacitance measurements were performed using an Oriel 3A solar simulator with neutral density filters of varying optical densities (0.1 to 4). Capacitance-voltage (C-V) and capacitance-frequency (C-F) measurements were carried out using SCS 4200 under dark and illumination. DC bias voltages from −1 to 1 V were swept along with a low frequency (10 kHz) ac signal (10 mV) for C-V measurement. Frequency-dependent capacitance of the devices were analyzed in the range of 10 kHz to 100 kHz under zero bias condition. J-V characteristics at different temperatures were done by placing the samples inside a cryostat. UV–vis absorption and photoluminescence (PL) spectra of ZnO film were acquired using a SHIMADZU UV-3600 spectrophotometer and HORIBA Jobin Yvon Nanolog Spectrofluorometer respectively.

Results and discussion

For a better understanding of the optical properties of the ZnO layer with change in thickness, UV–vis and PL spectra were recorded. Figure 1(a) shows the UV–vis absorption spectra of the ZnO layer coated on a glass slide. The absorption spectra show a significant increase in absorbance value with negligible shifting of absorption band edge as the ZnO layer thickness is increased. The optical band gap determined using Tauc plot is found to be ∼3.5 eV for all the ZnO layer thicknesses as shown in the inset of figure 1(a) [17]. Transparency is one of the essential criteria to be considered while choosing ETL in an inverted solar cell since the active layer should receive the maximum visible light. The transmittance spectra of ZnO film of different thicknesses are shown in figure 1(b). All the films transmit ∼97% of the visible light (400 nm–700 nm) whereas the transmittance in the UV region decreases with the increase of ZnO layer thickness. Figure 1(c) shows the room temperature PL spectra of ZnO film of different thicknesses at an excitation wavelength of 330 nm. Typically, the PL spectra of ZnO consist of two peaks- one in the UV region and another in the visible region (green emission). The emission peak in the UV region around 385 nm is due to the near band edge transition of ZnO [18]. The visible region peak around 580 nm corresponds to the deep level or trap state emission [19]. In our case, the green emission is stronger than the UV emission (figure 1(c)). The ratio of UV emission intensity to green emission intensity was found to be 0.78, 0.50, 0.33 and 0.18 for ZnO layer thicknesses of 30, 70, 150 and 250 nm respectively. The high intensity ratio of 30 nm thick ZnO layer can be attributed to fewer defects and higher crystallinity of the film [20].

The energy band diagram of the inverted device structure ITO/ZnO/PTB7:$PC_{71}BM$/MoO_3/Ag is given in the supplementary material (figure S1 is available online at stacks.iop.org/MRX/5/116203/mmedia). Figure 2(a) shows the J-V characteristics of the inverted devices with different thickness of ZnO layer. The increase in the thickness of the ZnO layer reduces the J_{sc} and V_{oc} values of the devices and which in turn directly

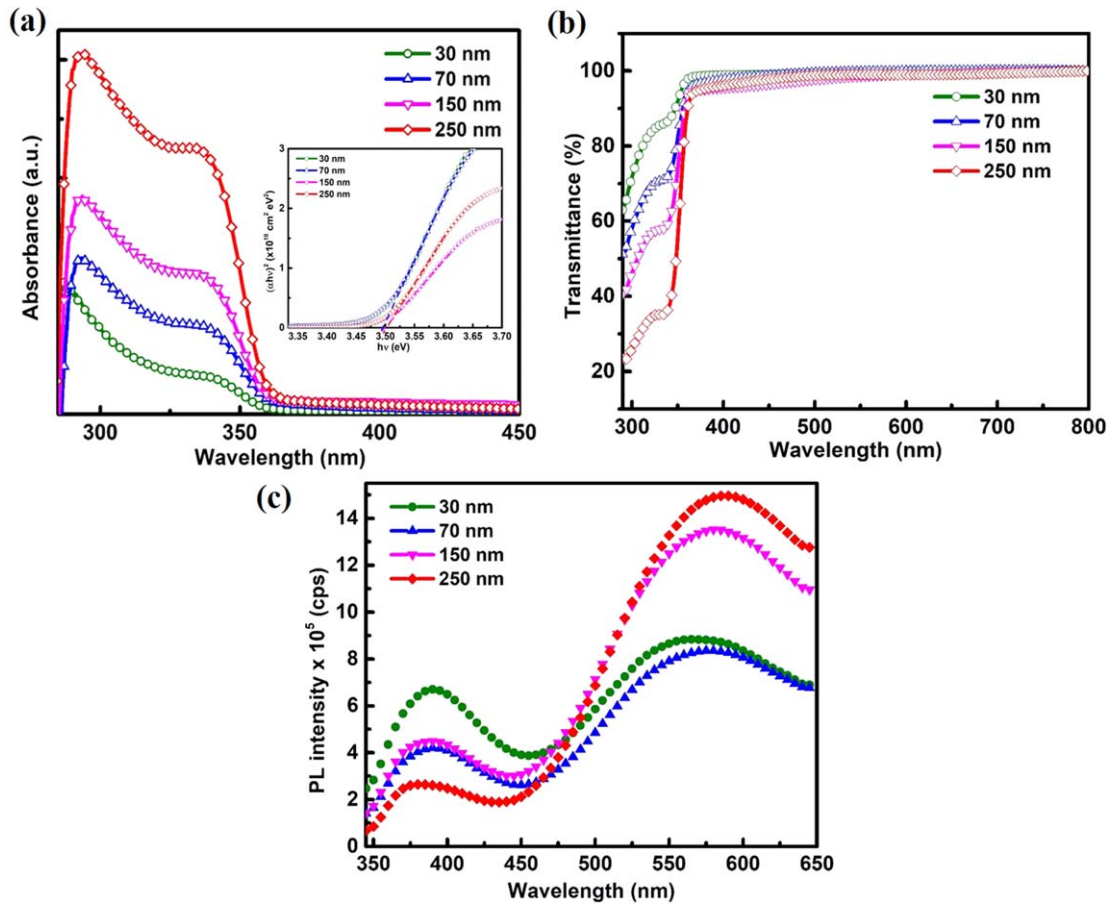

Figure 1. Optical properties of ZnO films (a) UV–vis absorption spectra with Tauc plot in the inset and (b) transmission spectra of different thicknesses of ZnO layer. (c) Room temperature photoluminescence spectra of varying ZnO layer thicknesses excited at 330 nm.

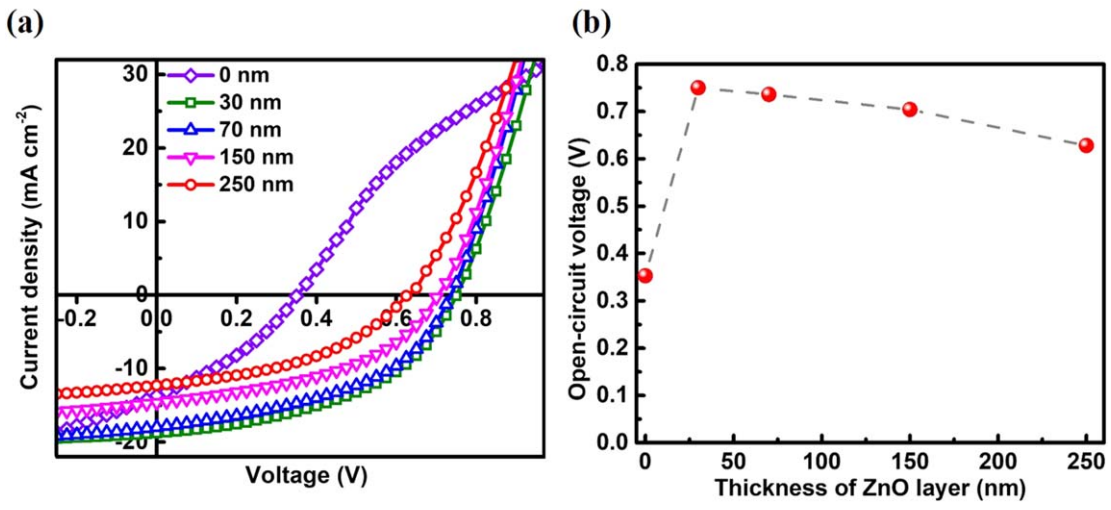

Figure 2. Device performance under 1-sun illumination (a) J-V curves of PTB7:$PC_{71}BM$ inverted devices for different thicknesses of ZnO layer. (b) The open-circuit voltage dependence on the ZnO layer thickness.

affects the power conversion efficiency. The cell parameters obtained from the J-V characteristics are tabulated (table S1 in the supplementary material). The device without ZnO layer shows a low V_{oc} of 0.375 V, and on increasing the ZnO layer thickness from 30 to 250 nm, theV_{oc} decreased from 0.750 to 0.628 V (figure 2(b)). Variation in V_{oc} can be due to charge accumulation at the interfaces. Intensity-dependent capacitance measurements provide insight into the trap states at the interfaces [21]. Capacitance as a function of frequency

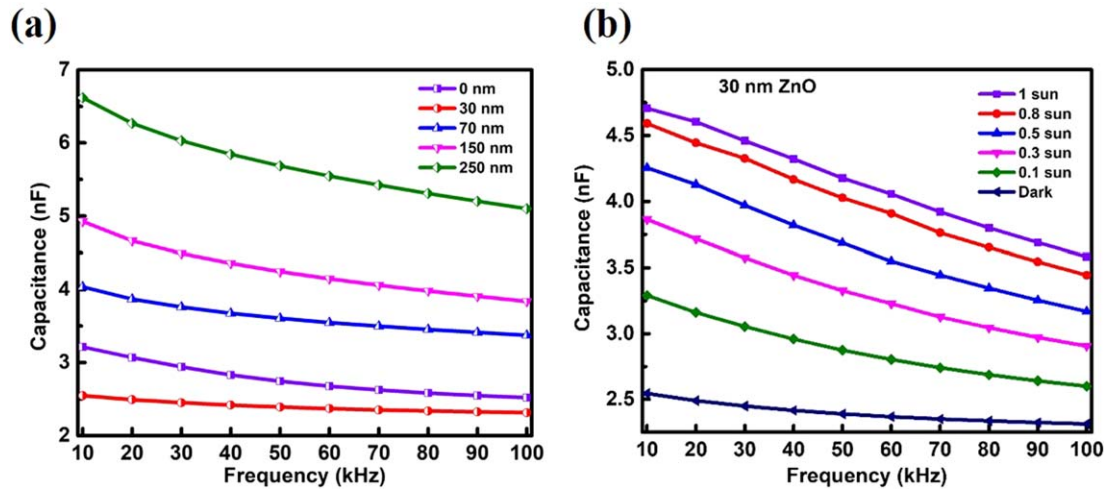

Figure 3. Capacitance-Frequency characteristics (a) Capacitance as a function of frequency for different thicknesses of ZnO layer under dark (b) Intensity-dependent capacitance as a function of frequency for 30 nm ZnO layer.

(C-F) is measured under dark on devices of different thicknesses of ZnO layer indicates an increase of capacitance with a decrease in frequency (figure 3(a)). However, for a particular frequency, the capacitance value increases with the thickness of ZnO layer. Figure 3(b) shows the light intensity-dependent capacitance as a function of frequency for device with 30 nm thick ZnO layer. It is observed that capacitance increases with increase in the illumination intensity. Capacitance measurements provide information about the electric field arrangement inside a device. Trap capacitance and depletion capacitance contribute towards the total capacitance [22]. The traps in the active layer and interfaces influence the trap capacitance [23]. Trapped charges can vary the electric field inside the device and thereby increase the capacitance value. At low frequency, charges from deep trap states contribute towards the increased capacitance [21]. The increase in capacitance with ZnO thickness can be correlated to the trap states present at the interface. Light intensity dependent C-F plots for the devices with 70, 150 and 250 nm ZnO layer thicknesses are given in the supplementary material (figure S2).

Photoinduced capacitance-voltage (C-V) study is a useful tool to investigate the charge accumulation at the interface. C-V measurements for different illumination intensities are performed for devices with varying ZnO layer thicknesses. The light intensity was varied from 20 to 80 mW cm^{-2} using neutral density filters, of varying optical densities. Figure 3(b) shows the C-V characteristics of the device with 30 nm thick ZnO layer. As the bias voltage swept from negative to a positive value, the capacitance value increases initially indicating an enhancement of charge accumulation at the interface. At a particular voltage, $V_{C\text{-}peak}$, the capacitance value becomes maximum due to the injection of charges. With the further increase of bias voltage beyond $V_{C\text{-}peak}$, the capacitance value falls off due to the recombination of injected charges with photogenerated charge carriers [24]. The $V_{C\text{-}peak}$ values are observed to be 0.55, 0.50 and 0.48 V for devices with ZnO layer thicknesses 30, 70 and 150 nm respectively (figures 4(a)–(c)). The reduction in the $V_{C\text{-}peak}$ value with the increase in ZnO layer thickness is an indication of increased accumulation of charges at the interface [11, 25]. For a device with particular thickness of ZnO layer, there is a shift in the $V_{C\text{-}peak}$ value as the illumination intensity is varied from 1 sun to 0.2 sun. This $V_{C\text{-}peak}$ shift can be correlated with the amount of charge accumulation. Larger the shift, higher the accumulation of charge carriers at the interface [26]. For devices with 30 nm thick ZnO layer, the $V_{C\text{-}peak}$ shift is observed to be 0.05 V whereas the shift for 70 and 150 nm devices are 0.15 and 0.16 V respectively. Thus it is evident that the amount of charge accumulation increases as the ZnO layer thickness increases. On the contrary, in the case of 250 nm ZnO layer device, the $V_{C\text{-}peak}$ value (0.19 V) is found to be invariant with illumination intensity (figure 4(d)). It can be due to the inefficient electron transport property of 250 nm thick ZnO layer [11].

Light intensity-dependent J-V characteristics enable to identify different recombination mechanisms in the system. Considering only the Langevin recombination in a polymer: fullerene solar cell, V_{oc} of the device can be expressed as [27],

$$V_{oc} = \frac{E_g}{q} - \frac{kT}{q} \ln\left(\frac{(1-P)\gamma N_c^2}{PG}\right) \quad (1)$$

where E_g is the effective bandgap, G is the exciton generation rate, P is the probability of exciton dissociation, γ is the Langevin recombination constant, and N_c is the density of states. P and γ are intensity independent parameters whereas G is directly proportional to light intensity. A slope of kT/q obtained from the V_{oc} versus

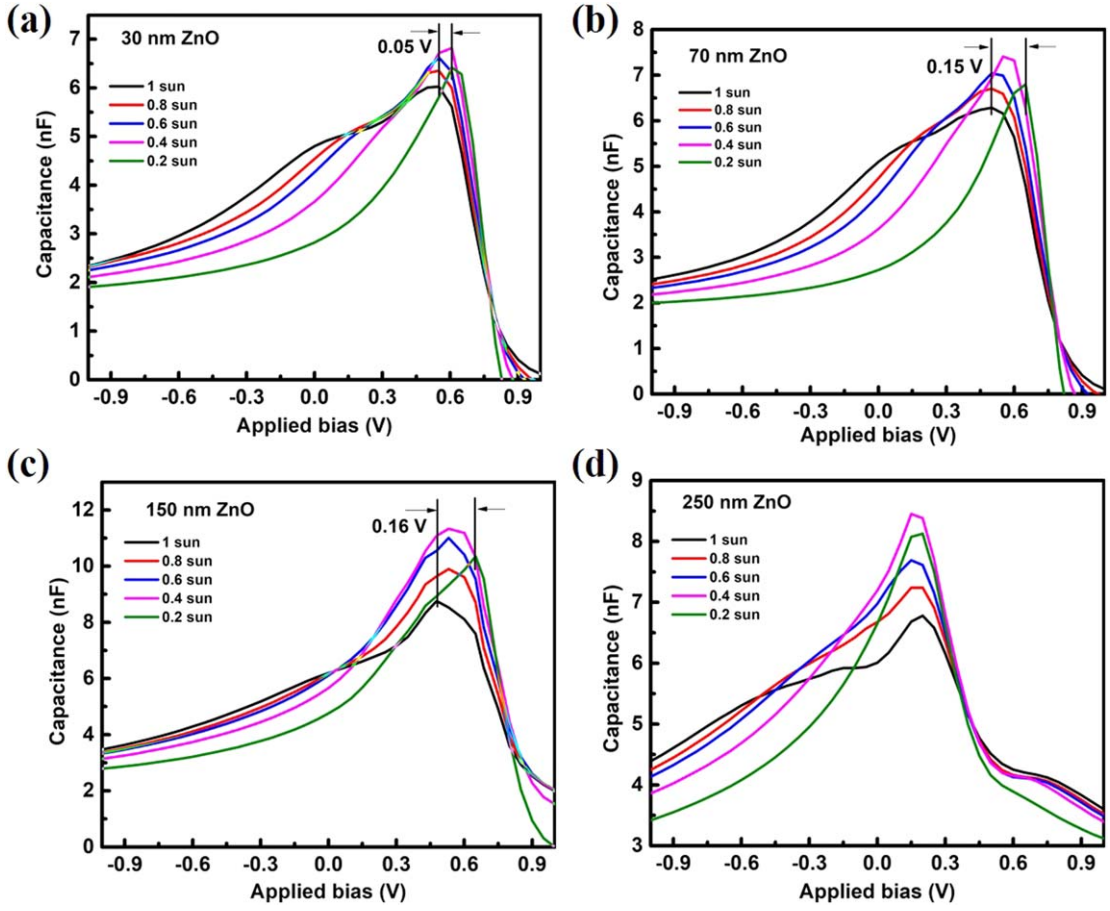

Figure 4. Intensity-dependent Capacitance-Voltage measurement for (a) 30 nm ZnO layer device, (b) 70 nm ZnO layer device, (c) 150 nm ZnO layer device and (d) 250 nm ZnO layer device.

light intensity curve indicates the absence of trap-assisted recombination [27]. Trap-assisted Shockley-Read-Hall recombination is monomolecular recombination where a hole and an electron recombine via localized energy trap [28]. From figure 5(a), the slope of V_{oc} vs light intensity curve for the devices with 30 and 70 nm thick ZnO layer are calculated to be 0.97 kT/q and 1.22 kT/q respectively. Whereas the values are 2.43 kT/q and 3.84 kT/q for 150 and 250 nm ZnO layer devices respectively, showing the dominance of trap-assisted recombination. The large deviation of the slope from kT/q can also be due to the effect of leakage current. Light intensity dependent FF analysis can give a clear picture of leakage current. Unlike photocurrent, the leakage current is independent of illumination intensity. A decrease in FF with the reduction of light intensity implies that photocurrent is affected by the leakage current [29]. Figure 5(b) shows the intensity dependence of FF for all the devices. For the 30 nm thick ZnO device, initially, the FF increases with a decrease in light intensity and then remains constant. In such cases, the effect of leakage current can be discarded. A similar trend is observed for 70 nm thick ZnO device also. In the other two devices (150 and 250 nm), the FF reduces as the light intensity decreases. The rate of decrease is high for the 250 nm ZnO device which shows a strong influence of leakage current. In the low intensity region, 0 nm thick ZnO device also shows a similar trend as 150 nm and 250 nm thick ZnO devices. Unlike other devices, the 0 nm thick ZnO device shows a different behavior at higher intensities. Fill factor decreases as the light intensity increases. This is caused due to the nongeminate recombination in the device [30]. As observed in figure 2(a), the J-V curve of the device without ZnO layer (0 nm) shows an S-shaped behavior. Such behavior is due to the formation of a potential barrier for charge collection at the metal-organic interface which will reduce the charge collection and promote recombination [31]. As the intensity of light increases, more photogenerated charges are created which will promote recombination thereby reducing the fill factor at higher intensities. The presence of leakage current can be correlated with the shunt resistance (R_{sh}) values obtained from the dark J-V curve (table S1 in the supplementary material). The R_{sh} value is found to be decreasing as the thickness of the ZnO layer increases which increases leakage current. The J_{sc} dependence on the light intensity will give an insight about the bimolecular recombination in the device and is provided by the power law, $J_{sc} \propto I^{\alpha}$, where α is a scaling exponent [28]. As observed in figure 5(c), the value of α is ~1 for all the devices indicating a small loss due to bimolecular recombination.

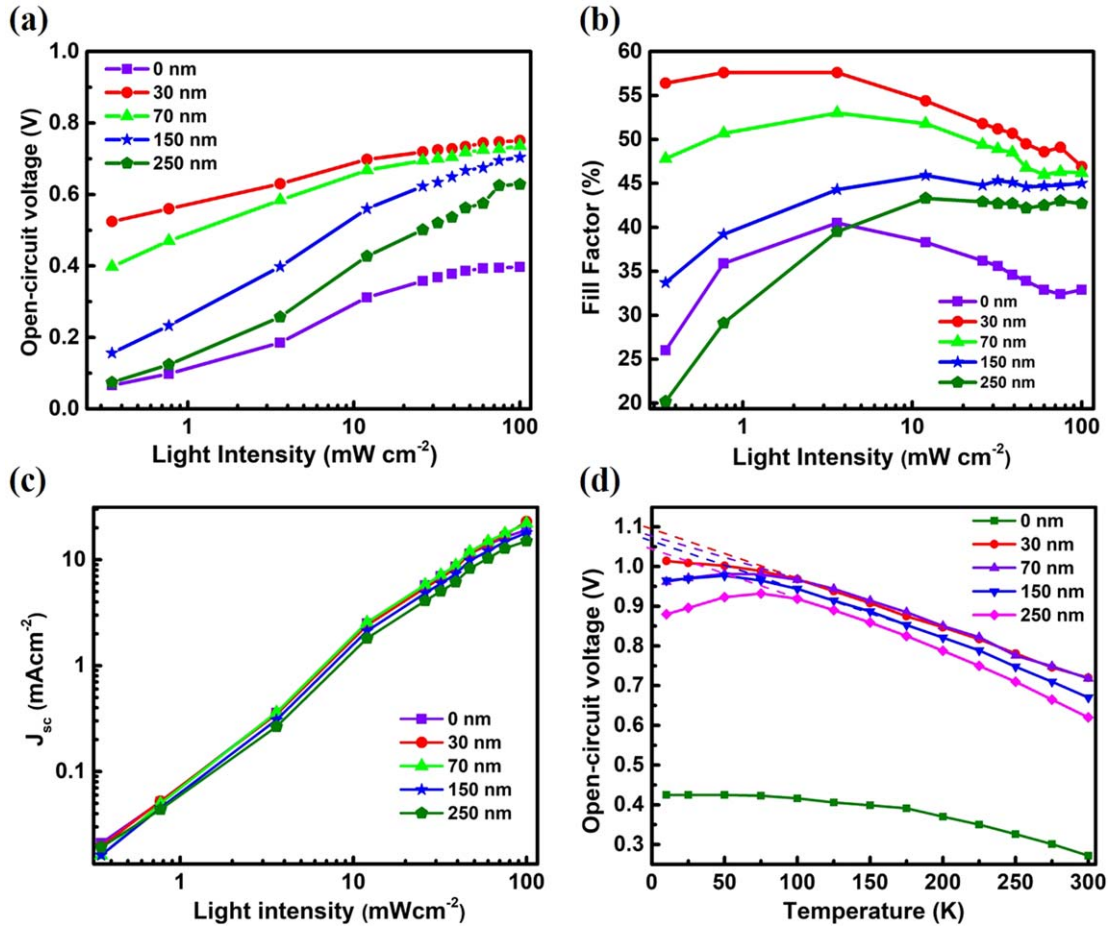

Figure 5. Illumination intensity dependence on (a) open-circuit voltage (b) fill factor and (c) short-circuit current for different thickness of ZnO layer. (d) Open-circuit voltage is plotted as a function of temperature for devices with varying ZnO layer thicknesses.

Another important parameter governing the device performance is the built-in potential (V_{bi}). It affects the device's internal electric field and limits the open circuit voltage [32]. V_{bi} can be determined from the temperature dependent V_{oc} measurement. V_{oc} can be expressed in terms of density of states as [33],

$$qV_{oc} = E_g - k_B T \ln\left(\frac{N_c N_v}{np}\right) \tag{2}$$

where E_g is the effective band gap, $n(p)$ is the electron (hole) concentration, N_c (N_v) is the effective conduction band (valence band) density of states and k_BT is the thermal energy. The temperature coefficient of V_{oc} can be expressed as [34],

$$\frac{dV_{oc}}{dT} \approx \frac{dE_g/q}{dT} + \frac{V_{oc} - E_g/q}{T} \tag{3}$$

where E_g is the effective band gap. In equation (3), the second term can be correlated to the temperature dependence of V_{oc}. On integrating, a linear relation is obtained as $V_{oc} \propto T^{-1}$. V_{oc} increases as the temperature decreases, and at lower temperatures, it saturates or slightly decreases. The constant value of voltage at lower temperature corresponds to V_{bi} [35]. From the temperature dependent V_{oc} plot, the effective band gap, E_g, can be determined by extrapolating the high temperature region of the curve towards the V_{oc} axis at zero Kelvin while an extrapolation of the low temperature region gives V_{bi}. The temperature dependent V_{oc} curves given in figure 5(d) show saturation of V_{oc} at low temperatures for all the devices with different thicknesses of ZnO layer. Nevertheless, the device without ZnO layer (0 nm) shows V_{oc} saturation even at high temperatures. The saturation of V_{oc} at high temperatures can be ascribed to the increase of barrier height, resulting from non ohmic contact between the active layer and the electrode [32]. In such cases, extrapolation of V_{oc} curve to determine E_g can lead to incorrect values. The values of V_{bi} and E_g obtained for the devices with different thicknesses of ZnO layer are tabulated (table 1). The saturation of V_{oc} at low temperature is attributed to the effect of injection barriers created at the contacts rather than the bulk properties [32]. The sum of injection barriers at the contacts ($\phi_n + \phi_p$) can be evaluated using the relation [32],

Table 1. Effective band gap (E_g), *the* built-in potential (V_{bi}) and barrier height ($\phi_n + \phi_p$) of PTB7:$PC_{71}BM$ inverted bulk heterojunction device for different thicknesses of ZnO layer.

ZnO layer thickness (nm)	E_g (eV)	V_{bi} (V)	$\phi_n + \phi_p$ (eV)
30	1.09	1.02	0.07
70	1.07	0.98	0.09
150	1.06	0.96	0.10
250	1.04	0.92	0.12

$$qV_{oc} = E_g - (\phi_n + \phi_p) \tag{4}$$

where ϕ_n and ϕ_p are the electron and hole injection barriers respectively, E_g is the effective band gap determined from V_{oc} versus temperature plot. The values of ($\phi_n + \phi_p$), calculated using equation (4) (table 1), show an increment with increase of ZnO layer thickness. The increase of barrier height contributes significantly to the loss of open-circuit voltage which in turn affects the power conversion efficiency of the solar cells as evident from figure 2(a).

Conclusions

In summary, we have analyzed the effect of ZnO layer thickness on the photovoltaic properties of PTB7:$PC_{71}BM$ inverted bulk heterojunction solar cell. The ZnO layer thicknesses were varied from 30 to 250 nm. Compared to other ZnO layer thicknesses, 30 nm thick film showed better transparency with fewer defects as evident from the transmission and PL spectra. Devices fabricated using 30 nm ZnO layer exhibited high efficiency with improved V_{oc} and J_{sc} values. The reduced charge accumulation at the active layer/ZnO interface in the case of devices with 30 nm thick ZnO layer improved the V_{oc} value as comprehended from capacitance measurements. The thin ZnO layer (30 nm) effectively reduced the barrier height and thereby enhanced the J_{sc} value. The deterioration of the performance of the devices with increase of ZnO layer thickness can be attributed to the presence of trap-assisted recombination and leakage current.

Supplementary material

See supplementary material for the energy band diagram of the device, C-F measurements, the photovoltaic parameters of all the devices and the calculation of optical band gap from Tauc plot of different ZnO layers,.

Acknowledgments

The authors acknowledge financial support from the Solar Energy Research Initiative (Department of Science and Technology, Government of India), Ministry of Human Resource Development (Government of India), and Indian Institute of Science Education and Research Thiruvananthapuram (IISER TVM), Kerala, India.

ORCID iDs

Manoj A G Namboothiry https://orcid.org/0000-0003-4839-8065

References

[1] Heeger A J 2014 25th anniversary article: bulk heterojunction solar cells: understanding the mechanism of operation *Adv. Mater.* **26** 10–28
[2] He Z, Zhong C, Su S, Xu M, Wu H and Cao Y 2012 Enhanced power-conversion efficiency in polymer solar cells using an inverted device structure *Nat Photonics* **6** 591
[3] Mohan M *et al* 2017 Efficient organic photovoltaics with improved charge extraction and high short-circuit current *J. Phys. Chem.* C **121** 5523–30
[4] Zuo L, Yu J, Shi X, Lin F, Tang W and Jen A K Y 2017 High-efficiency nonfullerene organic solar cells with a parallel tandem configuration *Adv. Mater.* **29** 1702547
[5] Brabec C J *et al* 2001 Origin of the open circuit voltage of plastic solar cells *Adv. Funct. Mater.* **11** 374–80
[6] Qi B and Wang J 2012 Open-circuit voltage in organic solar cells *J. Mater. Chem.* **22** 24315–25
[7] Elumalai N K and Uddin A 2016 Open circuit voltage of organic solar cells: an in-depth review *Energy Environ. Sci.* **9** 391–410
[8] Scharber M C *et al* 2006 Design rules for donors in bulk-heterojunction solar cells—towards 10% energy-conversion efficiency *Adv. Mater.* **18** 789–94
[9] Ramsdale C, Barker J, Arias A, MacKenzie J, Friend R H and Greenham N 2002 The origin of the open-circuit voltage in polyfluorene-based photovoltaic devices *J. Appl. Phys.* **92** 4266–70
[10] Vandewal K, Tvingstedt K, Gadisa A, Inganäs O and Manca J V 2010 Relating the open-circuit voltage to interface molecular properties of donor:acceptor bulk heterojunction solar cells *Phys. Rev.* B **81** 125204

[11] Zang H, Hsiao Y-C and Hu B 2014 Surface-charge accumulation effects on open-circuit voltage in organic solar cells based on photoinduced impedance analysis *Phys. Chem. Chem. Phys.* **16** 4971–6
[12] Motiei L *et al* 2010 Self-propagating molecular assemblies as interlayers for efficient inverted bulk-heterojunction solar cells *J. Am. Chem. Soc.* **132** 12528–30
[13] Seo J H, Kim H and Cho S 2012 Build-up of symmetry breaking using a titanium suboxide in bulk-heterojunction solar cells *Phys. Chem. Chem. Phys.* **14** 4062–5
[14] Sun Y, Seo J H, Takacs C J, Seifter J and Heeger A J 2011 Inverted polymer solar cells integrated with a low-temperature-annealed sol-gel-derived ZnO film as an electron transport layer *Adv. Mater.* **23** 1679–83
[15] Özgür Ü *et al* 2005 A comprehensive review of ZnO materials and devices *J. Appl. Phys.* **98** 11
[16] Liu D and Kelly T L 2014 Perovskite solar cells with a planar heterojunction structure prepared using room-temperature solution processing techniques *Nat. Photon.* **8** 133–8
[17] Viezbicke B D, Patel S, Davis B E and Birnie D P III 2015 Evaluation of the Tauc method for optical absorption edge determination: ZnO thin films as a model system *Phys. Status Solidi* B **252** 1700–10
[18] Kong Y, Yu D, Zhang B, Fang W and Feng S 2001 Ultraviolet-emitting ZnO nanowires synthesized by a physical vapor deposition approach *App Phys Lett* **78** 407–9
[19] Vanheusden K, Warren W L, Seager C H, Tallant D R, Voigt J A and Gnade B E 1996 Mechanisms behind green photoluminescence in ZnO phosphor powders *J. Appl. Phys.* **79** 7983–90
[20] Liu X, Wu X, Cao H and Chang R 2004 Growth mechanism and properties of ZnO nanorods synthesized by plasma-enhanced chemical vapor deposition *J. Appl. Phys.* **95** 3141–7
[21] Ray D, Burtone L, Leo K and Riede M 2010 Detection of trap charge in small molecular organic bulk heterojunction solar cells *Phys. Rev.* B **82** 125204
[22] Kesavan A V, Rao A D and Ramamurthy P C 2017 Interface electrode morphology effect on carrier concentration and trap defect density in an organic photovoltaic device *ACS Appl. Mater. Interfaces* **9** 28774–84
[23] Bisquert J, Garcia-Belmonte G, Munar A, Sessolo M, Soriano A and Bolink H J 2008 Band unpinning and photovoltaic model for P3HT: PCBM organic bulk heterojunctions under illumination *Chem. Phys. Lett.* **465** 57–62
[24] Garcia-Belmonte G, Munar A, Barea E M, Bisquert J, Ugarte I and Pacios R 2008 Charge carrier mobility and lifetime of organic bulk heterojunctions analyzed by impedance spectroscopy *Org Electron* **9** 847–51
[25] Zhao C, Chen B, Qiao X, Luan L, Lu K and Hu B 2015 Revealing underlying processes involved in light soaking effects and hysteresis phenomena in perovskite solar cells *Adv. Energy Mater.* **5** 1500279
[26] Cho S *et al* 2014 Role of additional PCBM layer between ZnO and photoactive layers in inverted bulk-heterojunction solar cells *Sci. Rep.* **4** 4306
[27] Koster L J A, Mihailetchi V D, Ramaker R and Blom P W 2005 Light intensity dependence of open-circuit voltage of polymer: fullerene solar cells *Appl. Phys. Lett.* **86** 123509
[28] Proctor C M, Kuik M and Nguyen T-Q 2013 Charge carrier recombination in organic solar cells *Prog. Polym. Sci.* **38** 1941–60
[29] Proctor C M and Nguyen T-Q 2015 Effect of leakage current and shunt resistance on the light intensity dependence of organic solar cells *App Phys Lett* **106** 23_21
[30] Brus V V, Proctor C M, Ran N A and Nguyen T Q 2016 Capacitance spectroscopy for quantifying recombination losses in nonfullerene small-molecule bulk heterojunction solar cells *Adv. Energy Mater.* **6** 1502250
[31] de Castro F A, Heier J, Nüesch F and Hany R 2010 Origin of the kink in current-density versus voltage curves and efficiency enhancement of polymer-C60 heterojunction solar cells *IEEE Journal of Selected Topics in Quantum Electronics* **16** 1690–9
[32] Rauh D, Wagenpfahl A, Deibel C and Dyakonov V 2011 Relation of open circuit voltage to charge carrier density in organic bulk heterojunction solar cells *Appl. Phys. Lett.* **98** 69
[33] Garcia-Belmonte G 2010 Temperature dependence of open-circuit voltage in organic solar cells from generation–recombination kinetic balance *Sol. Energy Mater. Sol. Cells* **94** 2166–9
[34] Würfel P 2005 *Physics of Solar Cells* (Weinheim: Wiley-VCH)
[35] Mingebach M, Deibel C and Dyakonov V 2011 Built-in potential and validity of the Mott-Schottky analysis in organic bulk heterojunction solar cells *Phys. Rev.* B **84** 153201